1 **Screening and identification of metacaspase inhibitors, evaluation of**

2 **inhibition mechanism and trypanocidal activity**

3 Brian Pérez[a], León A. Bouvier[a], Juan José Cazzulo[a], Fernán Agüero[a], Emir

4 Salas-Sarduy[a,#] and Vanina E. Alvarez[a,#]

5

6 [a] Instituto de Investigaciones Biotecnológicas "Dr. Rodolfo Ugalde"–

7 Universidad Nacional de San Martín – CONICET, San Martín, B1650HMP,

8 Buenos Aires, Argentina.

9

10 # Address correspondence to Vanina E. Alvarez,

11 vanina.eder.alvarez@gmail.com and Emir Salas-Sarduy,

12 emirsalas@gmail.com.

13

14 Running Head: Evaluation of trypanosomatid metacaspase inhibitors

15

Abstract

17 A common strategy to identify new antiparasitic agents is the targeting of
18 proteases due to their essential contribution to parasite growth and
19 development. Metacaspases (MCAs) are cysteine proteases present in fungi,
20 protozoa and plants. These enzymes, which are associated with crucial cellular
21 events in trypanosomes, are absent in the human host, thus arising as
22 attractive drug targets. To find new MCA inhibitors with trypanocidal activity, we
23 adapted a continuous fluorescent enzymatic assay to a medium-throughput
24 format and carried out screening of different compound collections, followed by
25 the construction of dose-response curves for the most promising hits. We used
26 MCA5 from *T. brucei* (*Tb*MCA5) as a model for the identification of inhibitors
27 from the GlaxoSmithKline HAT and CHAGAS chemical boxes. We also
28 assessed a third collection of 9 compounds from the Maybridge database
29 identified by virtual screening as potential inhibitors of the cysteine peptidase
30 falcipain-2 (Clan CA) from *Plasmodium falciparum*. Compound HTS01959 (from
31 the Maybridge collection) was the most potent inhibitor with IC_{50} of 14.39 μM;
32 also inhibiting other MCAs from *T. brucei* and *T. cruzi* (*Tb*MCA2=4.14 μM,
33 *Tb*MCA3=5.04 μM and *Tc*MCA5=151 μM). HTS01959 behaved as a reversible,
34 slow binding and noncompetitive inhibitor of *Tb*MCA2, with a mechanism of
35 action that included redox components. Importantly, HTS01959 displayed
36 trypanocidal activity against bloodstream forms of *T. brucei* and
37 trypomastigotes forms of *T. cruzi,* without cytotoxic effect on VERO cells. Thus,
38 HTS01959 is a promising starting point to develop more specific and potent
39 chemical structures to target MCAs.

Introduction

41 Parasite proteases comprise a large and diverse group of enzymes that, having

42 vital roles in nutrition and pathogenicity, offer great potential for drug

43 development. In the last few years, extensive research has been dedicated to a

44 unique family of enzymes called metacaspases (MCAs), which are cysteine

45 peptidases present in plants, fungi and protozoa (1). MCAs contain a His-Cys

46 catalytic dyad and have been classified into Clan CD according to their

47 structural homology with caspases (family C14), clostripain (family C11),

48 gingipain (family C25) and separase (family C50). Among the biochemical

49 similarities inside this clan, is the restricted specificity dominated by the nature

50 of the residue on the amino-terminal side of the scissile bond, which in the case

51 of MCAs is a basic amino acid residue (Arg or Lys) (2). MCAs are active as

52 monomers and do not require activation by proteolytic processing, but are

53 absolutely dependent on the presence of free calcium (usually at mM

54 concentrations) (3–5) to display maximal activity. Among the best-studied

55 MCAs are those present in trypanosomatids (6), parasitic protists that cause

56 serious neglected diseases in man and animals and affect a large number of

57 people worldwide. They include *Trypanosoma cruzi,* the etiological agent of

58 Chagas disease in South America, *Trypanosoma brucei* which causes African

59 sleeping sickness in humans and Nagana in animals and different species from

60 the genus *Leishmania* that produce diverse clinical forms of leishmaniasis.

61 The genome of *Trypanosoma brucei* encodes 5 metacaspase genes (*TbMCA1-*

62 *5*) (7). For *Tb*MCA2, the peptidase activity was experimentally confirmed (4), a

63 finding that can be extrapolated to the almost identical *Tb*MCA3. In addition,

64 and according to the presence of an intact catalytic dyad, *Tb*MCA5 can be

65 predicted to be active. In contrast, *Tb*MCA1 and *Tb*MCA4 have substitutions of

66 these residues and could lack peptidase activity, a fact that was demonstrated

67 for recombinant *Tb*MCA4 (8). Active *T. brucei* MCAs have stage regulated

68 expression, and are present mainly in mammalian (bloodstream) infective

69 forms, with only *Tb*MCA5 being additionally expressed at the insect (procyclic)

70 stage (9). It is interesting to note that a certain level of redundancy might exist

71 between different MCAs, since individual RNAi down-regulation does not affect

72 parasite growth in culture. However, simultaneous (triple) RNAi silencing leads

73 to a lethal phenotype, indicating that MCAs indeed play a crucial role in the cell

74 (9). In *Trypanosoma cruzi* on the other hand, there are 2 MCA paralogues

75 named *Tc*MCA3 and *Tc*MCA5, which are present in multiple copies and as a

76   single copy gene, respectively (10). Both types of genes encode for active
77   proteases that are tightly regulated, and from overexpression experiments a
78   role in cell death, cell cycle progression and differentiation have been inferred
79   (3). More recently, the DNA-damage inducible protein 1 (Ddi1) was identified as
80   a conserved natural metacaspase substrate (11). Ddi1 is a proteasomal shuttle
81   delivering proteins for degradation through the interaction with the proteasome
82   *via* their ubiquitin-like domain and at the same time with ubiquitinated cargoes
83   through their ubiquitin associated domain. Metacaspase cleavage eliminates
84   the UBA domain present in Ddi1 and reduces the protein stability, which in turn
85   could affect many diverse and important cellular processes including protein
86   degradation and cell cycle control.

87   MCAs hence arose as attractive potential drug targets due to their absence in
88   mammals, their low sequence similarity to human caspases and their
89   participation in diverse and important biological events. However, only a few
90   inhibitors were described to date based on the Arg specificity of these enzymes,
91   exhibiting micromolar inhibition and modest antiparasitic activity (12). Here, we
92   report the adaptation of a continuous fluorescent enzymatic assay to a medium-
93   throughput format to screen the GlaxoSmithKline HAT and CHAGAS boxes.
94   These boxes encompass 404 compounds with a great structural diversity and
95   exhibiting high antiparasitic potency and no toxicity for mammalian cells.
96   Interestingly, these molecules are novel (as they do not contain analogs to
97   drugs currently used for Chagas disease or sleeping sickness) and display
98   drug-like physicochemical properties (13). In addition, we assessed a third
99   collection of 9 compounds from the Maybridge database identified by virtual
100   screening as potential inhibitors of the cysteine peptidase falcipain-2 (Clan CA)
101   from *Plasmodium falciparum* (14). For the best resulting compound
102   (HTS01959), we further characterized the inhibition potency for multiple MCAs,
103   the inhibition mode, and finally evaluated the antiparasitic activity on *T. brucei*
104   and *T. cruzi* infective forms.

105

106   **Results**

107   **Development of a HTS-capable *Tb*MCA5 assay**

108   With the aim to screen larger compound collections we first developed and
109   optimized a continuous fluorogenic assay for *Tb*MCA5 using the prototypic
110   metacaspase substrate Z-VRPR-AMC (15). We carried out the optimization
111   process in solid-black 384 well plates, using a small set of bioactive

112   compounds. A convenient enzyme concentration in the assay was determined

113   through the activity of 2-fold dilutions of recombinant *Tb*MCA5 at a fixed

114   substrate concentration of 75 μM (Figure 1A). For all the enzyme

115   concentrations, progression curves remained linear for at least 40 minutes and

116   the Selwyn test (16) indicated that the enzyme remained stable during the

117   assay (R^2=0.994 for the linear fit of data from different enzyme concentrations

118   to a single curve) (Figure 1B). In addition, the V_0 vs. $[E]_0$ curve showed the

119   expected linear behavior for a wide range of enzyme concentrations (Figure

120   1C) and neither Triton X-100 (0-0.03% v/v) nor DMSO (0-3% v/v) induced

121   noticeable changes in enzyme activity (data not shown). Thus, we selected

122    $[TbMCA5]_0$=103 nM as the running enzyme concentration for the assay.

123   Surprisingly, the enzymatic activity of *Tb*MCA5 remained linear with respect to

124   Z-VRPR-AMC concentration in the range 7.81 μM – 1 mM, suggesting that

125   even the highest substrate concentration assayed was well below the K_M value

126   (Figure 1D). As it was impractical to use such a high substrate concentration for

127   the screening, we continued using a substrate concentration of 75 μM, although

128   it would hinder the identification of uncompetitive inhibitors. In the absence of

129   enzyme, no spontaneous hydrolysis of the Z-VRPR-AMC substrate was

130   observed; although some level of photobleaching was suggested by the linear

131   decay in fluorescent readouts with time. Although we were unable to reduce

132   further the moderate dispersion of enzyme positive controls (VC ≤ 12.5%), the

133   optimized assay exhibited a satisfactory performance during preliminary

134   characterization experiments, with a dynamic range (μ^{C+} - μ^{C-}) higher than 1200

135   RFU/sec, a μ^{C+}/μ^{C-} ratio ≥ 1000 and a Z' factor value around 0.6.

136   **Five compounds inhibit *Tb*MCA5 in a dose-dependent manner**

137   With the aim to identify new *Tb*MCA5 inhibitors active against *T. brucei* and *T.*

138   *cruzi*, we initially assessed the compound sets identified from high throughput

139   phenotypic screening against *T. brucei* (HAT box) and *T. cruzi* (CHAGAS box).

140   In addition, we also evaluated a small set of 9 compounds from the Maybridge

141   database, previously identified by us through structure-based virtual screening

5

142   as potential inhibitors of the cysteine peptidase falcipain-2 from *Plasmodium*

143   *falciparum* (17). All compounds were assayed in singlet (without technical

144   replicates) at a fixed dose of 33.3 μM due to the limited availability of stocks. As

145   shown in Figure 2, the vast majority of investigated compounds were inactive

146   on *Tb*MCA5 and those with activity, exhibited only modest inhibitory effects. At

147   the tested concentration,21 compounds reduced *Tb*MCA5 activity by 30% or

148   more. These compounds were included in the secondary screening. Statistics

149   for primary screening are summarized in Table S1.

150   To estimate IC_{50} for the resulting hits, two-fold serial dilutions (ranging from 125

151   μM to 3.8 pM) were analyzed using identical conditions, except for a reduction

152   in the assay volume to 40 μL to achieve higher compound concentrations. Of

153   the 21 hits selected during primary screening, only five showed dose-

154   dependent inhibition of *Tb*MCA5 (Figure 3A). Among them, 4 hits from the HAT

155   (TCMDC-143373, TCMDC-143382) and CHAGAS (TCMDC-143071, TCMDC-

156   143601) boxes showed modest IC_{50} values in the range 79-142 μM while the

157   compound HTS01959 from the Maybridge collection, was the most potent

158   *Tb*MCA5 inhibitor with an IC_{50} value of 12.6 μM (Figure 3, panel A). The

159   structures of the identified hits are depicted in Figure 3B.

160   **HTS01959 preferentially inhibits the metacaspases of *T. brucei***

161   Given that HTS01959 inhibited *Tb*MCA5 6 to 11 times more potently than the

162   rest of the identified inhibitors, we decided to functionally characterize this

163   inhibition in terms of modality and specificity. Initially, we investigated whether

164   HTS01959 was able to inhibit other closely related metacaspases. In addition to

165   *Tb*MCA5, HTS01959 inhibited metacaspases 2 and 3 (*Tb*MCA2 and 3) from *T.*

166   *brucei* (Figure 4A). Of note, this compound inhibited both enzymes more

167   potently than *Tb*MCA5, with similar IC_{50} values in the low micromolar range

168   (Table 2). Interestingly, metacaspases from other organisms, such as *Tc*MCA5

169   (*T. cruzi*) and Yca1 (*Saccharomyces cerevisiae*) were significantly less

170   sensitive to HTS01959 inhibition (Figure 4B).

171   We further expanded our specificity analysis to prototypical peptidases from

172   different mechanistic classes. As expected, HTS01959 was inactive against

173   non-related peptidases such as chymotrypsin (Class: Serine, Clan PA, family

174   S1), pepsin (Class: Aspartic, Clan AA, family A1) or angiotensin-1 converting

175   enzyme (Class: Metallo, Clan MA, family M2) and weakly active against the
176   papain-like cysteine peptidases cruzipain and falcipain-2 (Clan CA, family C1)
177   (Figure S1).

178   **HTS01959 behaves as a reversible, slow binding and**
179   **noncompetitive inhibitor of *Tb*MCA2.**

180   Considering that *Tb*MCA2 was the *T. brucei* metacaspase more potently
181   inhibited by HTS01959 and the only one whose crystallographic structure has
182   been determined (18), we decided to continue the characterization of
183   HTS01959 inhibitory activity using *Tb*MCA2 as model enzyme. Features of the
184   *Tb*MCA2 assay are summarized in Figure S2.

185   We next characterized HTS01959 in terms of reversibility and time dependence
186   of *Tb*MCA2 inhibition. Reversible interaction with the enzyme was verified by
187   the recovery of *Tb*MCA2 activity after rapid addition of substrate (100-fold jump
188   dilution) to the pre-incubated mix of enzyme and inhibitor (Figure 5A). In this
189   experiment, the compound displayed a linear progressive curve (Figure 5A)
190   with a stable inhibition value, indicative of rapid onset of steady state (i.e. rapid
191   dissociation of EI complex). In contrast, the inhibitor displayed a different kinetic
192   behavior when enzyme was added to a reaction mix previously containing
193   inhibitor and substrate (Figure 5B). In this case, HTS01959 showed non-linear
194   kinetics, with inhibition progressively increasing over time (time-dependent
195   inhibition). As stable inhibition was observed only after ~1 hour, all subsequent
196   kinetic experiments for this compound included preincubation (≥ 60 min at 37
197   ºC) with the enzyme.

198   To investigate the mode of inhibition of HTS01959 on the activity of *Tb*MCA2,
199   we evaluated the impact of substrate concentration on the apparent IC_{50} value
200   over the widest range ($0.04xK_M$ –$1.6xK_M$) of substrate saturations we could
201   assess. For this, we used a reduced set of four HTS01959 concentrations
202   selected to: (i) include IC_{50} value at each substrate condition and (ii) cover the
203   wider inhibition range (~10-90 %) in the central stretch of the dose-response

204   curve. As observed in Figures 5C and 5D, IC_{50} values decreased with the
205   increment of substrate concentration (Table S3), suggesting an apparent non-
206   competitive inhibition phenotype, with α<1. As complete Michaelis curves were
207   not obtained at each inhibitor concentration, we were unable to estimate
208   definitive values for α and Ki (Figure S3).

The inhibitory mechanisms of HTS01959 include a redox
component

211   Given that cysteine peptidases rely on the reduced state of their catalytic
212   sulfhydryl group for maximal enzymatic activity, they are particularly susceptible
213   to thiol-reactive compounds, which can reduce enzyme activity by several redox
214   mechanisms. In many cases, the activity of these compounds can be
215   significantly modified by changing the reduction potential of the activity buffer,
216   thus providing a diagnostic test to detect compound-specific redox effects (19).
217   To establish if this could be the case for HTS01959, we investigated the effect
218   of the strength and concentration of reducing agents on the inhibition of
219   TbMCA2 by this molecule. As shown in Figure 6A, the IC_{50} value increased
220   more than two orders of magnitude with the increment of DTT concentration (in
221   the range 0.1 - 20 mM) in the assay buffer, suggesting a dose-dependent
222   protective role of strong reducing agents on TbMCA2 activity. A decrease of
223   HTS01959 inhibition with the increment in DTT concentrations was also
224   observed for other cysteine proteases such as cruzipain and falcipain-2 (Table
225   S2).

226   A significant decrease in the inhibitory potency of HTS01959 was also observed
227   in the presence of Cys (monothiol), which is considered a weak reducing agent
228   in comparison to DTT (dithiol). Strikingly, Cys displayed a more potent
229   protection of TbMCA2 activity than DTT in a wide range of concentrations. At a
230   Cys concentration of 0.1 mM, the IC_{50} value was 34-fold higher than that of DTT
231   at the same concentration, and the ratio increased to ≅ 69-fold at 1 mM (Table
232   3). At 10 mM, Cys completely abolished the inhibitory activity of HTS01959 on
233   TbMCA2 while a still significant inhibition (IC_{50}=49.2 μM) was observed at
234   identical DTT concentration. Of note, β-mercaptoethanol (10 mM), another
235   monothiol considered a weak reducing agent, also protected TbMCA2 activity
236   from HTS01959 inhibition better than DTT, although less potently (≅6-fold) than
237   Cys (Figure 6B).

8

238   We reasoned that the apparent low efficacy of DTT in protecting TbMCA2
239   activity from HTS01959 inhibition would result from the balance of opposing
240   (protective vs pro-inhibitory) effects that would not occur in the presence of
241   weak reducing agents (which would show only protective effects). Given that
242   some compounds are able to undergo redox cycling in the presence of DTT
243   leading to the generation of the strong oxidizing agent H_2O_2, we decided to
244   evaluate whether this could be the case of HTS01959 using an HRPO-based
245   colorimetric assay (20). As shown in Figure 7A, a significant increase in OD_{505nm}
246   was observed when HTS01959 was incubated in the presence of DTT (2 mM),
247   but not Cys, suggesting the generation of H_2O_2 under enzymatic assay
248   conditions. Interestingly, the generation of H_2O_2 was very low at 10 mM DTT,
249   which is in agreement with our inhibition experiments and previous reports (20).
250   Additionally, the IC_{50} value of HTS01959 was 4-fold higher (64.4 μM) in the
251   presence of the very efficient H_2O_2 decomposing enzyme catalase (Figure 7B).
252   This finding suggests that the generation of H_2O_2 operates as one of the
253   previously suspected pro-inhibitory mechanisms that specifically occur in the
254   presence of DTT. Of note, this also suggests that HTS01959 promotes
255   additional inhibitory effects on TbMCA2 activity independent of H_2O_2 generation,
256   as catalytically competent catalase concentrations were unable to abolish the
257   inhibitory activity of this compound.

258   **HTS01959 is active on *T. brucei* bloodstream forms and *T. cruzi***
259   **cell-derived trypomastigotes**

260   Finally, we evaluated the antiparasitic potential of HTS01959 in cultures of *T.*
261   *brucei* and *T. cruzi*. We estimated the half-maximal effective concentration
262   (EC_{50}) for this compound on *T. brucei* bloodstream forms by using the resazurin
263   viability assay. As shown in Figure 8A, HTS01959 reduced the growth in a
264   dose-dependent manner, with an EC_{50} value of 37.89 μM. In the case of *T.*
265   *cruzi*, HTS01959 was not effective against the replicative intracellular
266   amastigote form, as judged by the results obtained in our image-based assays
267   (Figure 8B); but exhibited a modest activity against the cell-derived
268   trypomastigote stage with a EC_{50} value of 91.2 μM determined by a resazurin
269   viability assay. Of note, HTS01959 cytotoxicity on Vero cells was negligible at
270   the highest concentration assayed (130 μM) using the highly sensitive
271   luminescent Cell viability assay CellTiter-Glo.

272   **Discussion**

9

273   Metacaspases have proven to be important in trypanosomatid parasites. These
274   enzymes have been involved in processes such as differentiation, cell cycle
275   progression, and protein homeostasis, all critical for parasite development and
276   survival (3–5, 9, 10, 21). Given the global incidence (22–24) of these parasites
277   and the absence of metacaspases in humans, they arise naturally as interesting
278   drug targets, which have been previously used for structure-based design of
279   bioactive inhibitors (12).

280   We exploited the availability of a generic fluorogenic substrate and our previous
281   experience in the exploration of GSK CHAGAS and HAT chemical boxes
282   against different targets, to identify new anti-metacaspase inhibitory scaffolds
283   bearing significant antiparasitic activity. Four hits, each one representing a
284   different inhibitory scaffold, were identified from both boxes. Although their
285   inhibitory potency against metacaspases (79-142 μM) was too modest to fully
286   explain their reported trypanocidal activity in culture (0.4-1 μM against their
287   respective parasites) (13), these confirmed hits might be structurally optimized
288   to increase their potency, considering that the crystallographic structure of
289   *Tb*MCA2 has been previously determined (18). Interestingly, two of these
290   compounds (TCMDC-143071 and TCMDC-143382) were also identified in a
291   previous work as micromolar inhibitors of the Zn-dependent M32
292   metallocarboxypeptidases *Tc*MCP-1 and *Tb*MCP-1 (25), suggesting the
293   possibility of a combined mode of action in these parasites (polypharmacology).

294   Although the assessment of the antiparasitic activity of investigated compounds
295   prior to their target-based evaluation is desirable (13), the most potent
296   metacaspase inhibitor identified by us in this work was not previously explored
297   in phenotypic screenings against trypanosomatid parasites. In the case of
298   HTS01959, the target-based approach led directly to the discovery of a hit that
299   simultaneously inhibited several metacaspases in the single-digit micromolar
300   range, showed a suitable enzyme inhibition profile and modest activity against
301   *T. brucei* and *T. cruzi* parasites with no apparent toxicity to Vero cells.

302   This compound displays a unique inhibition phenotype, characterized by
303   reversible effects on metacaspase activity, rapid dissociation from the enzyme
304   and time-dependent inhibition. Notably, HTS01959 inhibits *Tb*MCA2 non-
305   competitively, being to the best of our knowledge the first metacaspase inhibitor
306   displaying this feature. As all the inhibitors in this class, HTS01959 is expected
307   to be able to bind both the free enzyme and the enzyme-substrate complex,

10

308   although this compound seems to exhibit a higher affinity for the latter. More
309   importantly, this suggests that HTS01959 may target a binding pocket relatively
310   distant from the active site. From a medicinal chemistry perspective, the
311   identification and targeting of non-active (i.e., allosteric) binding sites within
312   enzyme molecules provides an attractive and effective alternative to traditional
313   active site-directed inhibitors, which might exhibit advantageous properties (i.e.,
314   selectivity). Regarding the difference observed in the inhibition for the *Tc*MCA5
315   enzyme, it is important to note that the sequence identity between *Tc*MCA5 and
316   *Tb*MCA5 catalytic domains is very high, and close to 75% while these enzymes
317   differ considerably at the C-terminal end with a sequence identity of
318   approximately 18% (See Fig S4 and S5). Taking into account that the
319   compound HTS01959 behaves as a non-competitive inhibitor, and thus exerts
320   its effect outside the active site, one possible explanation is that the divergent
321   C-terminal end might contribute to the different susceptibility of *Tc*MCA5 to this
322   molecule.

323   Possibly, the most prominent functional characteristic of HTS01959 is its ability
324   to generate, *in vitro*, H_2O_2 in the presence of strong reducing agents.
325   Retrospectively, this compound showed several hallmark features of redox
326   cycling compounds, such as time-dependent inhibition and an inhibitory
327   potency dependent on the strength and concentration of the reducing agent
328   used (20). Preliminary estimations showed that ~360 μM of H_2O_2 was
329   generated by 100 μM of HTS01959 in the assay buffer (containing 2 mM DTT)
330   during 1 hour at 37 ºC (Figure 7A). It is expected that such an amount of H_2O_2
331   could cause a significant effect on enzymatic activity of a wide variety of protein
332   targets. For that reason, redox cycling compounds are often presented as false-
333   positive hits or, at least, as nonspecific artifacts able to interfere with different
334   assays and target types (20). However, not all the cysteine peptidases assayed
335   in this study (and not even metacaspases) displayed a similar degree of
336   susceptibility to HTS01959. This suggests that a specific component exists and
337   that H_2O_2 is just one of the inhibitory mechanisms exhibited by this compound.
338   In addition, the contribution of this mechanism to the global inhibitory activity of
339   HTS01959 sharply decreases when DTT concentration rises to 10 mM, while a
340   significant inhibition is still apparent at least for *Tb*MCA2 (IC_{50}=49 μM). Finally,
341   the addition of catalase does not eliminate HTS01959 activity, confirming that
342   H_2O_2 generation was not the only inhibitory mechanism present. Taken
343   together, our results indicate that the effect of HTS01959 on metacaspase

11

344   activity, under the specific and non-physiological conditions assayed here, is
345   complex and multi-component.

346   From a chemical point of view, the functional groups present in a molecule
347   define the spectra of chemical reactions in which it might be involved within
348   living cells. In the case of HTS01959, the three ketonic carbonyl groups stand
349   out from the structure for their polar nature and reactivity, which can undergo
350   nucleophilic addition and redox reactions, among others (26, 27). From this fact,
351   several chemical mechanisms can be envisaged to explain part of the
352   antitrypanosomal activity observed for this compound. Some routes of direct
353   consumption of essential reducing power (NADH, NADPH or trypanothione) by
354   HTS01959 are depicted in Figure S6. It has been shown that the carbonyl
355   group of 9-Fluorenone can be reduced *in vivo* by the NADPH cytochrome P-
356   450 reductase or other dehydrogenases belonging to the short-chain
357   dehydrogenase/reductase (SDR) family (28, 29). Interestingly, we have found
358   several genes encoding functional SDR enzymes in *T. brucei* and *T. cruzi*
359   (Table S4), raising the possibility of such a conversion in trypanosomatid
360   parasites. Carbonyl groups in the 1,3 Indandione moiety might also be reduced
361   by a similar mechanism. In addition, indirect routes of oxidative stress might be
362   induced by the compound itself through the formation of intra- or intermolecular
363   disulfides and sulfenic acids in proteins. In such cases, different redox enzymes
364   within the parasite could cooperate to regenerate proteins to their reduced
365   forms *via* different trypanothione-consuming routes (30, 31)(32). Even the
366   enzyme-dependent generation of highly reactive oxygen species by HTS01959
367   (e.g. H_2O_2, organic hydroperoxides, etc) within the cell cannot be dismissed (33,
368   34). Finally, it is also possible that trypanothione, which at physiological pH is
369   partially in the de-protonated thiolate form and can act as a nucleophile (32), be
370   conjugated to carbonyl carbon(s) in HTS01959 by diverse trypanosomatid thiol-
371   transferase enzymes.   Independently of the specific reaction, all of these
372   mechanisms converge in the same final output which is to disrupt the vital
373   redox balance within the parasites.

374   Noteworthy, a number of trypanocidal drugs in clinical use (such as
375   benznidazole, nifurtimox, fexinidazole, melarsoprol and eflornithine) actually
376   interfere with antioxidant defenses, confirming the potential of this approach
377   (35, 36). Thus, a shortage in redox supply, caused by genetic or
378   pharmacological means, could increase the antiparasitic potency of HTS01959.

12

379   This not only suggests a route to experimentally validate our hypothesis, but
380   also raises the possibility to design drug combinations displaying synergistic
381   effects (i.e. with drugs that enhance parasite sensitivity to oxidative stress or
382   that increase the demand of redox defenses) (37).

383   In summary, HTS01959 represents an interesting compound displaying a
384   unique inhibitory mechanism toward validated trypanosomatid target enzymes.
385   Although the efficacy *in vivo* is moderate, the absence of cytotoxicity for
386   mammalian cells together with the potential for chemical optimization, further
387   encourage additional research to transform this compound into a more suitable
388   candidate.

389

390   **Materials and methods**

391   **Reagents:** Triton X-100, NaCl, TrisHCl, 4-(2-hydroxyethyl)-1-
392   piperazineethanesulfonic acid (HEPES), Dimethyl Sulfoxide (DMSO),
393   Dithiothreitol (DTT), Phenylmethylsulfonyl fluoride (PMSF), Resazurin,
394   Arabinose, Catalase and Black solid bottom polystyrene Corning® NBS 384-
395   well plates were purchased from Sigma-Aldrich.

396   **Cloning, expression and purification of MCAs**

397   All MCAs genes were cloned from the corresponding genomes by PCR in
398   pGEM T easy (Promega), fused with Glutathione S-transferase tag and then
399   subcloned into the expression vector pBAD as described previously (11) The
400   oligonucleotides used in the cloning by PCR of *Tb*MCA2 and *Tb*MCA3 genes
401   were as follows:

402   *Tb*MCA2 Sense Primer: AAGCTTCATATGTGCTCCTTAATTACACAACTC

403   *Tb*MCA3 Sense Primer: AAGCTTCATATGGCCGTGGACCCAAGGTG

404   *Tb*MCA2-3 Antisense Primer: ACTAGTTTGGATAGATCTGTCAACAGAAAAC

405   Expression of recombinant MCAs in *Escherichia coli* Bl21 Codon Plus (DE3)
406   strain and their purification via glutathione-sepharose resin were performed as
407   previously described (11). Recombinant protein expression levels in a soluble
408   form are considerably higher for *Tb*MCA2 and *Tb*MCA3 than for *Tb*MCA5.
409   Regarding the profiles obtained after purification, a major band corresponding

13

410   to the full-length proteins can be observed for *Tb*MCA2 and *Tb*MCA3 while for

411   *Tb*MCA5 the pattern is more complex with the presence of multiple self-

412   processing products, similar to what has been described for the orthologous

413   proteins of *Leishmania major* (38) and *T. cruzi* (3).

414   After purification, *T. brucei* metacaspases were changed to Activity Buffer

415   (HEPES 50 mM pH 8.0, 0.01% v/v Triton X-100, DTT 2 mM, $CaCl_2$ 0.8 mM) by

416   using PD-10 desalting columns (GE Healthcare) and incubated 3h at 37 ℃ for

417   pre-activation before storage at 4 ℃.

418   **Optimization of metacaspase enzymatic assay**

419   Metacaspase activities were assayed fluorometrically with Z-VRPR↓AMC

420   (GenScript) as substrate in HEPES 50 mM pH 8.0, DTT 2 mM, supplemented

421   with 0.01% v/v Triton X-100 (39) and different $CaCl_2$ concentrations (10 mM for

422   Yca1 and 0.8 mM for trypanosomatid metacaspases

423   *Tb*MCA2/*Tb*MCA3/*Tb*MCA5/*Tc*MCA5). Assays (final reaction volume 40 or 60

424   μL) were performed at 37 ℃ in solid black 384 well plates (Corning) at fixed

425   enzyme concentrations, as determined by titration with the irreversible inhibitor

426   Z-VRPR-FMK (GenScript) (40). Except when stated otherwise, fluorogenic

427   substrate was added at a final concentration of 75 μM. The release of AMC (7-

428   amino-4methylcoumarin) was monitored continuously for 30-60 min with a

429   FilterMax F5 Multimode Microplate Reader (Molecular Devices) using a

430   standard 360 nm excitation and 465nm emission filter set. Enzyme activity was

431   estimated as the slope (dF/dt) of the linear region of the resultant progress

432   curves. Under the described conditions, metacaspases activity showed no

433   significant changes in the presence of DMSO (0–3% v/v) and were completely

434   abolished by 10 mM EDTA.

435   The performance of the developed assay was estimated by the Z factor

436   parameter (41) using 16 replicates of enzyme (*Tb*MCA5 with DMSO) and

437   inhibition (*Tb*MCA5 with 10 μM of Z-VRPR-FMK) controls according to the

438   following equation:

439    $Z\ Factor = 1 - \frac{3(\sigma_p + \sigma_n)}{|\mu_p - \mu_n|}$

440   **Equation 1**

441   Where μ_p and μ_n are the average of positive and negative controls, respectively;

442   and σ_p and σ_n are the standard deviation of each control group.

443 **Compound collections**

444 GlaxoSmithKline HAT and CHAGAS boxes (13) were received as 10 mM stock
445 solutions in DMSO. For primary screening, a working solution (final
446 concentration of 2 mM) for each compound was prepared by 1/5 dilution in
447 DMSO while 1 µL of the 10 mM stock solution was used for secondary
448 screening of selected compounds (42). Nine compounds from Maybridge
449 database, previously identified by virtual screening as potential inhibitors of the
450 cysteine peptidase falcipain-2 (Clan CA) from *Plasmodium falciparum* (14),
451 were also assessed (stock solution 25 mM in DMSO). Working solutions at
452 2 mM and 10 mM in DMSO were prepared for primary and secondary screening
453 assays, respectively.

454 **Primary screening**

455 To perform primary screening, 1 µL of each compound (2 mM in DMSO), Z-
456 VRPR-FMK (10 µM in DMSO) or DMSO (negative controls) were dispensed
457 into 384-well Corning black solid-bottom assay plates. Then, 30 µL of Activity
458 Buffer 1X containing *Tb*MCA5 (103 nM final concentration in the assay) were
459 added to each well, the plates were agitated and each well subjected to a single
460 autofluorescence read ($\lambda_{ex/em}$ = 360/465 nm). Plates were incubated in darkness
461 for 1 hour at 37 °C in a wet chamber and then 30 µL of activity buffer containing
462 Z-VRPR-AMC (75 µM final concentration) were added to each well to start the
463 reaction. After agitation, the fluorescence of AMC was acquired kinetically for
464 each well (12 read cycles, one cycle every 300 seconds). Considering our
465 previous experiences (25, 42), the auto-fluorescent cut-off was arbitrarily set at
466 5×10^6 RFU to discard highly interfering compounds. All compounds were
467 assayed in singlet (without replicates) due to the limited availability of stocks.

468 Raw screening measurements were used to determine the slope (dF/dt) of
469 progression curves by linear regression for control and compound wells.
470 Percentage of inhibition (%Inh) was calculated for each compound according to
471 Equation 2:

472 $$\% \, Inhibition = 100 * \left[1 - \frac{\left(\frac{dF^{WELL}}{dT} - \mu^{C-} \right)}{(\mu^{C+} - \mu^{C-})} \right]$$ **Equation 2**

473 where dF/dt^{WELL} represents the slope of each compound well and μ^{C+} and μ^{C-}

474 the average of *Tb*MCA5 (no-inhibition) and substrate (no-enzyme) controls,

475 respectively.

476 **Secondary assay (dose-response curves)**

477 Twenty-one compounds showing more that 30% of inhibition were selected

478 from primary screening and re-tested in a dose-response manner (final

479 concentration ranging from 125 μM to 3.8 pM) using identical assay conditions

480 except 40 μL final volume instead of 60 μL. One μL of compound stocks (10

481 mM in DMSO) and Z-VRPR-FMK (10 mM in DMSO) were added to the first well

482 on row 1, followed by addition of 30 μL of Activity Buffer. After addition of 15 μL

483 of the same buffer to subsequent wells, 2-fold serial dilutions were made. Then

484 15 μL of activity buffer containing *Tb*MCA5 were added to each well, except for

485 those corresponding to C−; which were completed with 15 μL of activity buffer.

486 After agitation, 60 minutes of incubation at 37 °C and autofluorescence

487 measurement, 10 μL of Activity Buffer containing Z-VRPR-AMC substrate was

488 added to the mix. Data collection and processing were performed exactly as

489 described above. Percentage of *Tb*MCA5 residual activity was calculated for

490 each condition according to Equation 3:

491 $$\% \, Residual \; Activity = 100 * \left[\frac{\left(\frac{dF^{WELL}}{dT} - \mu^{C-} \right)}{(\mu^{C+} - \mu^{C-})} \right]$$ **Equation 3**

492 where dF/dt^{WELL} represents the slope of each compound well and μ^{C+} and μ^{C-}

493 the average of enzyme (no-inhibition) and substrate (no-enzyme) controls,

494 respectively. The IC$_{50}$ and Hill slope parameters for each compound were

495 estimated by fitting the four-parameter Hill equation to experimental data from

496 dose-response curves using the GraphPad Prism program (version 5.03).

497 **Specificity assay with prototypic enzymes from different mechanistic**

498 **classes**

499 Cruzipain (EC 3.4.22.51) and falcipain-2 (MEROPS ID: C01.046) were obtained

500 and assessed as previously described (17, 25). Purified rabbit lung ACE (EC

501 3.4.15.1) was purchased from Sigma-Aldrich and evaluated as described (43).

502 Chymotrypsin (EC 3.4.21.1) and Pepsin (EC 3.4.23.1) were commercially

503 obtained (Sigma-Aldrich) and assessed according to manufacturer instructions.

504 The substrates, inhibitors and wavelengths used are summarized in Table 1.

16

505 **Determining reversibility and mode of inhibition**

506 Reversibility and time dependence of *Tb*MCA2 inhibition by HTS01959 was
507 assayed as previously described (44). In brief, HTS01959 (200 µM; ~50 x IC_{50})
508 and *Tb*MCA2 (770 nM; ~100 x optimal assay concentration) were incubated at
509 37 ºC for 60 min in the activity buffer. The mix was 100-fold diluted into 40 µL of
510 Z-VRPR-AMC (75 µM in activity buffer) pre-incubated at the same temperature
511 in a 384-well plate. Immediately after mixing, AMC fluorescence ($\lambda_{ex/em}$ =
512 360/465 nm) was continuously monitored every minute for 1 hour. Z-VRPR-
513 FMK (40 nM; ~20 x IC_{50}) was used as a control for irreversible inhibition. For
514 *Tb*MCA2 control, the equivalent volume of DMSO vehicle was preincubated
515 with the enzyme.

516 To determine the kinetics of inhibition onset, *Tb*MCA2 (7.7 nM final
517 concentration) was added to a reaction mix (40 µL final volume) previously
518 equilibrated at 37 ºC containing activity buffer, HTS01959 (50 µM) and Z-
519 VRPR-AMC (75 µM). Immediately after mixing, AMC release was monitored as
520 indicated above.

521 The mode of inhibition of HTS01559 was determined as previously described
522 (17). In brief, *Tb*MCA2 activity was determined for at least six different substrate
523 concentrations (ranging from 62.5 µM to 2.5 mM) in the absence and presence
524 of a reduced set (four) of HTS01959 concentrations selected to: (i) include IC_{50}
525 value at each substrate condition and (ii) cover the wider inhibition range (~10-
526 90 %) in the central stretch of the dose-response curve. Data were rearranged
527 to estimate the percentage of *Tb*MCA2 residual activity for each condition and
528 the values for IC_{50} and Hill slope were estimated by fitting experimental data to
529 the four-parameter Hill equation by using GraphPad Prism.

530 **Effect of redox Potential in the inhibition of *Tb*MCA2 by HTS01959**

531 To analyze the effect of redox potential in the inhibitory activity of HTS01959,
532 dose-response curves were constructed for at least 8 inhibitor concentrations
533 as described above. Assays were performed in activity buffer containing
534 different concentrations of DTT (0.1–20 mM), L-cysteine (0.1–10 mM) or beta-
535 mercaptoethanol (10 mM). Resultant dose-response curves were fitted as
536 previously indicated to estimate the value of IC_{50} and Hill slope.

537 **Hydrogen peroxide generation Assay**

17

538   To detect the formation of hydrogen peroxide we used a commercial kit for

539   glycemia test (Wiener lab) following instructions from the manufacturer. Briefly,

540   samples were incubated as indicated to (potentially) generate H_2O_2. Resultant

541   H_2O_2 reacts with 4-aminofenazone and 4-hydroxybenzoate in the presence of

542   horseradish peroxidase to form red quinonimine. The increase in absorbance at

543   505 nm was measured with a FilterMax microplate reader.

544   **Mammalian cells culture**

545   Vero cells were grown at 37 °C in a 5% CO_2 humidified atmosphere using MEM

546   (Gibco), supplemented with 10% v/v fetal bovine serum (Natocor), 10 µg/mL

547   streptomycin (Sigma), and 100 U/mL penicillin (Sigma).

548   **Effect of HTS01959 on *T. brucei* bloodstream form**

549   *T. brucei* parasites were added to black 96-well plates (half-area) to a final

550   density of 10.000 parasites/mL (125 µL final volume) in HMI-9 medium

551   supplemented with G418 antibiotic (2 µg/mL), 10% v/v fetal bovine serum (FBS)

552   and containing different concentrations of HTS01959 (up to 130 µM) or DMSO

553   (up to 0.5% v/v). Cultures were incubated for 72 hours at 37 °C in 5% CO_2. For

554   viability detection, 12.5 µL of 10x resazurin sodium salt (Sigma-Aldrich) in

555   phosphate buffered saline was added to each well (final concentration 44 µM)

556   and plates were incubated for other 5 hours in darkness. The fluorescence of

557   the resorufin product was determined (λ_{exc}=530-570 nm; λ_{ems}= 590-620 nm)

558   using a FilterMax microplate reader. Raw measurements were normalized by

559   using 0.5% v/v DMSO and 50 µM Nifurtimox controls (100% and 0% viability,

560   respectively) to estimate the percentage of viability for each condition to

561   construct dose-response curves. The value for IC_{50} was estimated by fitting

562   experimental data to the four-parameter Hill equation by using GraphPad

563   Prism.

564   **Effect of HTS01959 on *T. cruzi* trypomastigotes**

565   Cell-derived *T. cruzi* trypomastigotes were cultured by passages in Vero cells at

566   37°C and 5% CO_2 humidified atmosphere in MEM (Gibco Life Technologies)

567   supplemented with 10% v/v fetal bovine serum, 10 µg/mL streptomycin, 100

568   U/mL penicillin. For dose-response curves, samples enriched in

569   trypomastigotes were obtained by the swimming-up method (45). Parasite

570   suspension (125 µL at $8x10^6$ parasites/mL) was added to black 96 well-plates

571   (half area) and incubated O.N. at 37 °C in 5% CO_2 with different concentrations

18

572   of HTS01959 (ranging from 16 µM up to 130 µM) or DMSO (up to 0.5% v/v).

573   After incubation, viability for each condition was estimated with resazurin, as

574   described above.

575   ***Trypanosoma cruzi* intracellular imaging assay**

576   To evaluate the effect of HTS01959 on amastigote replication, 10.000 Vero

577   cells/well were seeded in a 24-multiwell plate. After 48 h of growth, cells were

578   infected with *T. cruzi* trypomastigotes at a MOI of 100 for 4 hours. Then,

579   trypomastigotes were removed by medium aspiration and fresh medium

580   containing 130 µM HTS01959 was added. After 48 h incubation, samples were

581   fixed with 4% v/v paraformaldehyde and stained with 4′,6-diamidino-2-

582   phenylindole (DAPI, 100 µg/mL) for 1 hour. After a final wash with PBS the

583   coverslips were mounted with FluorSave reagent. Samples were observed by

584   microscopy with a Nikon Eclipse 80i microscope, and 30 photos were taken for

585   each sample using a 40x objective. Images were analyzed using ImageJ to

586   identify Vero cell nuclei and parasite nuclei/ kinetoplasts. The total number of

587   Vero cells, the number of infected cells and the number of amastigotes per

588   Vero cell were compared by using GraphPad Prism.

589

590 **References**

591   1.   Uren AG, O'Rourke K, Aravind LA, Pisabarro MT, Seshagiri S, Koonin EV,

592   Dixit VM. 2000. Identification of paracaspases and metacaspases: two

593   ancient families of caspase-like proteins, one of which plays a key role in

594   MALT lymphoma. Mol Cell 6:961–967.

595   2.   Minina EA, Staal J, Alvarez VE, Berges JA, Berman-Frank I, Beyaert R,

596   Bidle KD, Bornancin F, Casanova M, Cazzulo JJ, Choi CJ, Coll NS, Dixit

597   VM, Dolinar M, Fasel N, Funk C, Gallois P, Gevaert K, Gutierrez-Beltran

598   E, Hailfinger S, Klemenčič M, Koonin EV, Krappmann D, Linusson A,

599   Machado MFM, Madeo F, Megeney LA, Moschou PN, Mottram JC,

600   Nyström T, Osiewacz HD, Overall CM, Pandey KC, Ruland J, Salvesen

601   GS, Shi Y, Smertenko A, Stael S, Ståhlberg J, Suárez MF, Thome M,

602   Tuominen H, Van Breusegem F, van der Hoorn RAL, Vardi A, Zhivotovsky

603   B, Lam E, Bozhkov PV. 2020. Classification and Nomenclature of

604   Metacaspases and Paracaspases: No More Confusion with Caspases.

605   Mol Cell 77:927–929.

606 3. Laverrière M, Cazzulo JJ, Alvarez VE. 2012. Antagonic activities of
607   Trypanosoma cruzi metacaspases affect the balance between cell
608   proliferation, death and differentiation. Cell Death Differ 19:1358–1369.

609 4. Moss CX, Westrop GD, Juliano L, Coombs GH, Mottram JC. 2007.
610   Metacaspase 2 of Trypanosoma brucei is a calcium-dependent cysteine
611   peptidase active without processing. FEBS Lett 581:5635–5639.

612 5. Watanabe N, Lam E. 2011. Calcium-dependent activation and autolysis of
613   Arabidopsis metacaspase 2d. J Biol Chem 286:10027–10040.

614 6. Alvarez VE, Niemirowicz GT, Cazzulo JJ. 2013. Metacaspases,
615   autophagins and metallocarboxypeptidases: potential new targets for
616   chemotherapy of the trypanosomiases. Curr Med Chem 20:3069–3077.

617 7. Mottram JC, Helms MJ, Coombs GH, Sajid M. 2003. Clan CD cysteine
618   peptidases of parasitic protozoa. Trends Parasitol 19:182–187.

619 8. Proto WR, Castanys-Munoz E, Black A, Tetley L, Moss CX, Juliano L,
620   Coombs GH, Mottram JC. 2011. Trypanosoma brucei metacaspase 4 is a
621   pseudopeptidase and a virulence factor. J Biol Chem 286:39914–39925.

622 9. Helms MJ, Ambit A, Appleton P, Tetley L, Coombs GH, Mottram JC. 2006.
623   Bloodstream form Trypanosoma brucei depend upon multiple
624   metacaspases associated with RAB11-positive endosomes. J Cell Sci
625   119:1105–1117.

626 10. Kosec G, Alvarez VE, Agüero F, Sánchez D, Dolinar M, Turk B, Turk V,
627   Cazzulo JJ. 2006. Metacaspases of Trypanosoma cruzi: possible
628   candidates for programmed cell death mediators. Mol Biochem Parasitol
629   145:18–28.

630 11. Bouvier LA, Niemirowicz GT, Salas-Sarduy E, Cazzulo JJ, Alvarez VE.
631   2018. DNA-damage inducible protein 1 is a conserved metacaspase
632   substrate that is cleaved and further destabilized in yeast under specific
633   metabolic conditions. FEBS J 285:1097–1110.

634 12. Berg M, Van der Veken P, Joossens J, Muthusamy V, Breugelmans M,
635   Moss CX, Rudolf J, Cos P, Coombs GH, Maes L, Haemers A, Mottram JC,
636   Augustyns K. 2010. Design and evaluation of Trypanosoma brucei
637   metacaspase inhibitors. Bioorg Med Chem Lett 20:2001–2006.

638 13. Peña I, Pilar Manzano M, Cantizani J, Kessler A, Alonso-Padilla J,
639   Bardera AI, Alvarez E, Colmenarejo G, Cotillo I, Roquero I, de Dios-Anton
640   F, Barroso V, Rodriguez A, Gray DW, Navarro M, Kumar V, Sherstnev A,
641   Drewry DH, Brown JR, Fiandor JM, Julio Martin J. 2015. New compound

642   sets identified from high throughput phenotypic screening against three
643   kinetoplastid parasites: an open resource. Sci Rep 5:8771.

644 14. Hernández-González JE, Salas-Sarduy E, Hernández Ramírez LF,
645   Pascual MJ, Álvarez DE, Pabón A, Leite VBP, Pascutti PG, Valiente PA.
646   2018. Identification of (4-(9H-fluoren-9-yl) piperazin-1-yl) methanone
647   derivatives as falcipain 2 inhibitors active against Plasmodium falciparum
648   cultures. Biochim Biophys Acta Gen Subj 1862:2911–2923.

649 15. Vercammen D, Belenghi B, van de Cotte B, Beunens T, Gavigan J-A, De
650   Rycke R, Brackenier A, Inzé D, Harris JL, Van Breusegem F. 2006.
651   Serpin1 of Arabidopsis thaliana is a suicide inhibitor for metacaspase 9. J
652   Mol Biol 364:625–636.

653 16. Selwyn MJ. 1965. A simple test for inactivation of an enzyme during
654   assay. Biochim Biophys Acta 105:193–195.

655 17. Alberca LN, Chuguransky SR, Álvarez CL, Talevi A, Salas-Sarduy E.
656   2019. In silico Guided Drug Repurposing: Discovery of New Competitive
657   and Non-competitive Inhibitors of Falcipain-2. Front Chem 7:534.

658 18. McLuskey K, Rudolf J, Proto WR, Isaacs NW, Coombs GH, Moss CX,
659   Mottram JC. 2012. Crystal structure of a Trypanosoma brucei
660   metacaspase. Proc Natl Acad Sci USA 109:7469–7474.

661 19. Thorne N, Auld DS, Inglese J. 2010. Apparent activity in high-throughput
662   screening: origins of compound-dependent assay interference. Curr Opin
663   Chem Biol 14:315–324.

664 20. Johnston PA. 2011. Redox cycling compounds generate H2O2 in HTS
665   buffers containing strong reducing reagents – real hits or promiscuous
666   artifacts? Curr Opin Chem Biol 15:174–182.

667 21. Vandana   null, Dixit R, Tiwari R, Katyal A, Pandey KC. 2019.
668   Metacaspases: Potential Drug Target Against Protozoan Parasites. Front
669   Pharmacol 10:790.

670 22. Prevention C-C for DC and. 2019. CDC - Chagas Disease - Epidemiology
671   & Risk Factors.

672 23. Prevention C-C for DC and. 2019. CDC - Leishmaniasis.

673 24. 2019. CDC - DPDx - Trypanosomiasis, African.

674 25. Salas-Sarduy E, Landaburu LU, Karpiak J, Madauss KP, Cazzulo JJ,
675   Agüero F, Alvarez VE. 2017. Novel scaffolds for inhibition of Cruzipain
676   identified from high-throughput screening of anti-kinetoplastid chemical
677   boxes. Sci Rep 7:12073.

678 26. Riant O, Hannedouche J. 2007. Asymmetric catalysis for the construction

21

679 of quaternary carbon centres: nucleophilic addition on ketones and
680 ketimines. Org Biomol Chem 5:873–888.

681 27. Goldberg K, Schroer K, Lütz S, Liese A. 2007. Biocatalytic ketone
682 reduction--a powerful tool for the production of chiral alcohols--part I:
683 processes with isolated enzymes. Appl Microbiol Biotechnol 76:237–248.

684 28. Chen C, Lefers RC, Brough EL, Gurka DP. 1984. Metabolism of alcohol
685 and ketone by cytochrome P-450 oxygenase: fluoren-9-ol in equilibrium
686 with fluoren-9-one. Drug Metab Dispos 12:421–426.

687 29. Habe H, Chung J-S, Kato H, Ayabe Y, Kasuga K, Yoshida T, Nojiri H,
688 Yamane H, Omori T. 2004. Characterization of the upper pathway genes
689 for fluorene metabolism in Terrabacter sp. strain DBF63. J Bacteriol
690 186:5938–5944.

691 30. Schlecker T, Comini MA, Melchers J, Ruppert T, Krauth-Siegel RL. 2007.
692 Catalytic mechanism of the glutathione peroxidase-type tryparedoxin
693 peroxidase of Trypanosoma brucei. Biochem J 405:445–454.

694 31. Budde H, Flohé L, Hecht H-J, Hofmann B, Stehr M, Wissing J, Lünsdorf H.
695 2003. Kinetics and redox-sensitive oligomerisation reveal negative subunit
696 cooperativity in tryparedoxin peroxidase of Trypanosoma brucei brucei.
697 Biol Chem 384:619–633.

698 32. Manta B, Bonilla M, Fiestas L, Sturlese M, Salinas G, Bellanda M, Comini
699 MA. 2018. Polyamine-Based Thiols in Trypanosomatids: Evolution, Protein
700 Structural Adaptations, and Biological Functions. Antioxid Redox Signal
701 28:463–486.

702 33. Forman HJ, Maiorino M, Ursini F. 2010. Signaling functions of reactive
703 oxygen species. Biochemistry 49:835–842.

704 34. Johnston PA. 2011. Redox cycling compounds generate H2O2 in HTS
705 buffers containing strong reducing reagents--real hits or promiscuous
706 artifacts? Curr Opin Chem Biol 15:174–182.

707 35. Caldas IS, Santos EG, Novaes RD. 2019. An evaluation of benznidazole
708 as a Chagas disease therapeutic. Expert Opin Pharmacother 20:1797–
709 1807.

710 36. Patterson S, Fairlamb AH. 2019. Current and Future Prospects of Nitro-
711 compounds as Drugs for Trypanosomiasis and Leishmaniasis. Curr Med
712 Chem 26:4454–4475.

713 37. A current analysis of chemotherapy strategies for the treatment of human
714 African trypanosomiasis. - PubMed - NCBI.

715 38. González IJ, Desponds C, Schaff C, Mottram JC, Fasel N. 2007.

716   Leishmania major metacaspase can replace yeast metacaspase in
717   programmed cell death and has arginine-specific cysteine peptidase
718   activity. Int J Parasitol 37:161–172.

719   39. Jadhav A, Ferreira RS, Klumpp C, Mott BT, Austin CP, Inglese J, Thomas
720   CJ, Maloney DJ, Shoichet BK, Simeonov A. 2010. Quantitative analyses
721   of aggregation, autofluorescence, and reactivity artifacts in a screen for
722   inhibitors of a thiol protease. J Med Chem 53:37–51.

723   40. Stennicke HR, Salvesen GS. 1999. Caspases: preparation and
724   characterization. Methods 17:313–319.

725   41. Zhang null, Chung null, Oldenburg null. 1999. A Simple Statistical
726   Parameter for Use in Evaluation and Validation of High Throughput
727   Screening Assays. J Biomol Screen 4:67–73.

728   42. Salas-Sarduy E, Landaburu LU, Carmona AK, Cazzulo JJ, Agüero F,
729   Alvarez VE, Niemirowicz GT. 2019. Potent and selective inhibitors for M32
730   metallocarboxypeptidases identified from high-throughput screening of
731   anti-kinetoplastid chemical boxes. PLoS Negl Trop Dis 13.

732   43. Carmona AK, Schwager SL, Juliano MA, Juliano L, Sturrock ED. 2006. A
733   continuous fluorescence resonance energy transfer angiotensin I-
734   converting enzyme assay. Nat Protoc 1:1971–1976.

735   44. Copeland RA. 2005. Evaluation of enzyme inhibitors in drug discovery. A
736   guide for medicinal chemists and pharmacologists. Methods Biochem Anal
737   46:1–265.

738   45. Ortega-Rodriguez U, Portillo S, Ashmus RA, Duran JA, Schocker NS,
739   Iniguez E, Montoya AL, Zepeda BG, Olivas JJ, Karimi NH, Alonso-Padilla
740   J, Izquierdo L, Pinazo M-J, de Noya BA, Noya O, Maldonado RA, Torrico
741   F, Gascon J, Michael K, Almeida IC. 2019. Purification of
742   Glycosylphosphatidylinositol-Anchored Mucins from Trypanosoma cruzi
743   Trypomastigotes and Synthesis of α-Gal-Containing Neoglycoproteins:
744   Application as Biomarkers for Reliable Diagnosis and Early Assessment of
745   Chemotherapeutic Outcomes of Chagas Disease. Methods Mol Biol
746   1955:287–308.

747

748

Legends to the Figures

Fig 1. Continuous fluorogenic assay for recombinant *Tb*MCA5. (A) Kinetic progression curves for different *Tb*MCA5 concentrations at a fixed dose (75 µM) of Z-VRPR-AMC. (B) Selwyn test for different *Tb*MCA5 concentrations. Data from different enzyme concentrations (represented by different symbols in the graph) are well fitted by a single curve. (C) Curve of V_0 vs. [*Tb*MCA5]$_0$. (D) Michaelis-Menten plot. In all cases, data corresponding to [*Tb*MCA5]=103 nM with [Z-VRPR-AMC]=75 µM, conditions selected for compound screening, are indicated in red. In panels C and D, V_0 is defined as the slope (dF/dt) of the linear region of progress (Fluorescence vs time) curves.

Fig 2. Activity plot for the assayed compounds during primary screening against *Tb*MCA5. The solid red line shows the average of enzyme activity controls (C+) and the solid green line represents the cutoff for selection of hits, which is 70% residual activity (equivalent to 30% inhibition). Open circles represent enzyme controls, closed black circles substrate controls, orange open circles inhibition controls (Z-VRPR-FMK). Blue and red triangles represent inactive compounds and hits, respectively. Highly auto-fluorescent compounds (17) were discarded from further analysis due to the negative impact they have on reproducibility (i.e. able to interfere significantly with fluorescence assay readouts).

Fig 3. Dose-response curves and structures of the identified *Tb*MCA5 inhibitors. (A) Dose-response curves. For each compound, the solid line represents the best fit of the four-parameter Hill equation to experimental data (open symbols). The best fit for the irreversible inhibitor Z-VRPR-FMK is represented in gray dotted line. Concentration of inhibitors (log, x-axis) is Molar. (B) Structures of identified *Tb*MCA5 inhibitors.

Fig 4. Dose-response curves for the inhibition of different metacaspases by HTS01959. (A) Dose-response curves for *T. brucei* metacaspases. (B) Dose-response curves for metacaspases from other organisms. For each curve, the solid line represents the best fit of the four-parameter Hill equation to experimental data (open figures). (C) Results summary of dose-response assays with different metacaspases incubated with HTS01959. HTS01959 concentration is expressed in M. ND: not determined.

24

782　**Fig 5. Reversibility and time dependence of the inhibition of *Tb*MCA2 by**
783　**HTS01959.** A) Product progress curves for the dissociation of E-I complex by
784　jumping dilution (100-fold) of enzyme-inhibitor mix into substrate solution. B)
785　Product progress curves for the formation of E-I complex by rapid addition of
786　the enzyme to a substrate-inhibitor mix. C) Dose-response curves of HTS01959
787　at increasing substrate concentrations. D) Effect of substrate concentration on
788　IC_{50} values. HTS01959 concentration is expressed in M.

789　**Fig 6. Effect of strength and concentration of reducing agents on the**
790　**inhibitory activity of HTS01959.** (A) Dose-response curves for the inhibition of
791　*Tb*MCA2 by HTS01959 at increasing concentrations of DTT. (B) Dose-
792　response curves in the presence of strong (DTT) and weak (β-mercaptoethanol
793　and cysteine) reducing agents at identical concentrations of 10 mM. For each
794　curve, the solid line represents the best fit of the four-parameter Hill equation to
795　experimental data (open figures). β-ME: β-mercaptoethanol. (C) Results
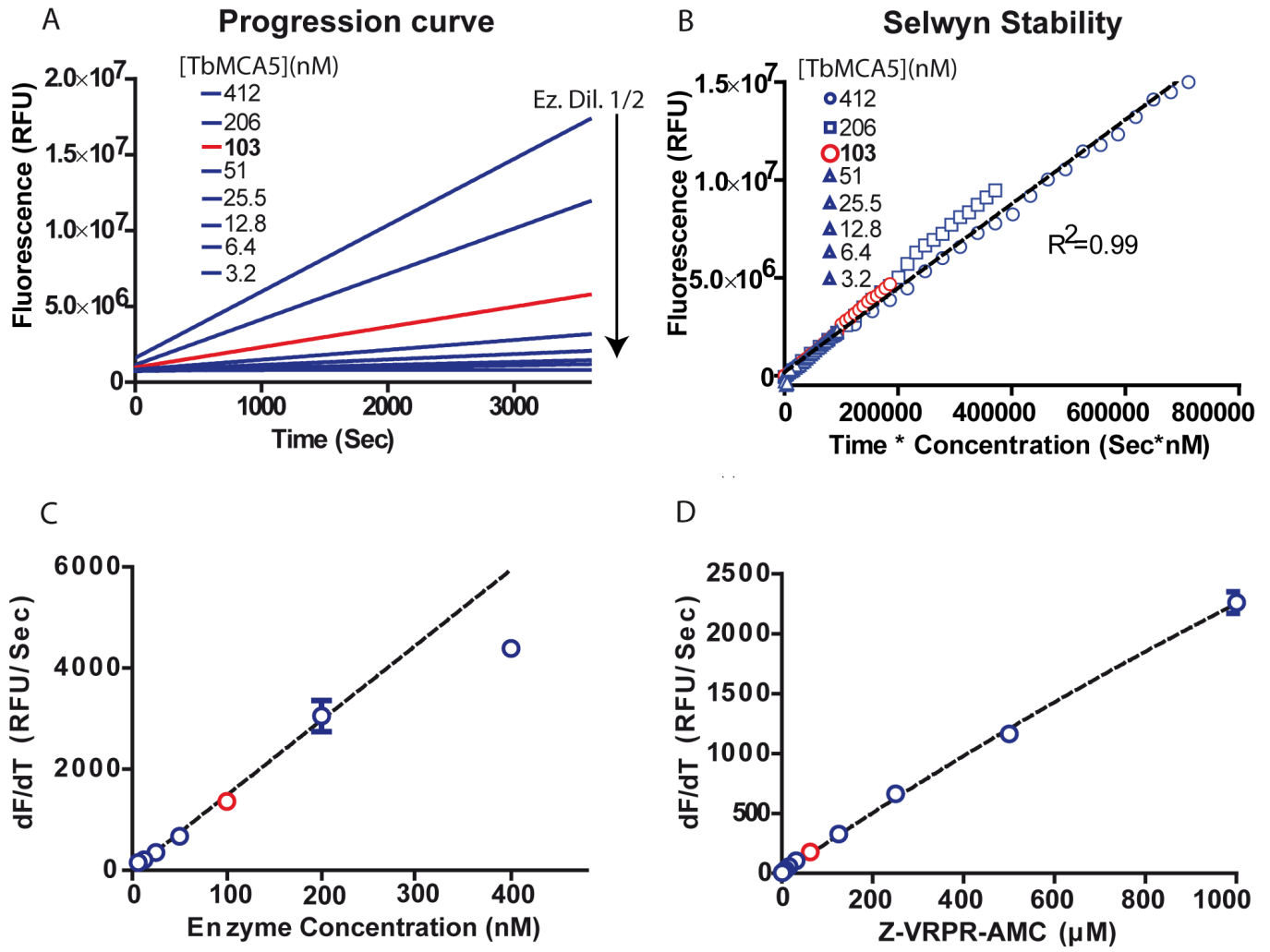796　summary of panel A and panel B. HTS01959 concentration is expressed in M.

797　**Fig 7. Specific hydrogen peroxide generation by HTS01959 in the**
798　**presence of low millimolar DTT concentrations. (**A) Enzymatic quantification
799　of H_2O_2 generated at different conditions by HRPO-catalyzed oxidation of 4-
800　aminophenazone. This reaction produces a colored product with strong
801　absorbance at 505 nm. C28 (2-hydroxy-3-(1-propenyl)-1,4-naphthoquinone) is
802　used as positive control of a quinoid Redox-cycling compound. The statistical
803　significance was evaluated by One-way anova and Tukey's multiple comparison
804　post test. Triple asterisk means p<0.001. (B) Dose-response curves for the
805　inhibition of *Tb*MCA2 by HTS01959 in the presence (200 μg/mL) and absence
806　of catalase. For each curve, the dotted line represents the best fit of the four-
807　parameter Hill equation to experimental data (open figures). HTS01959
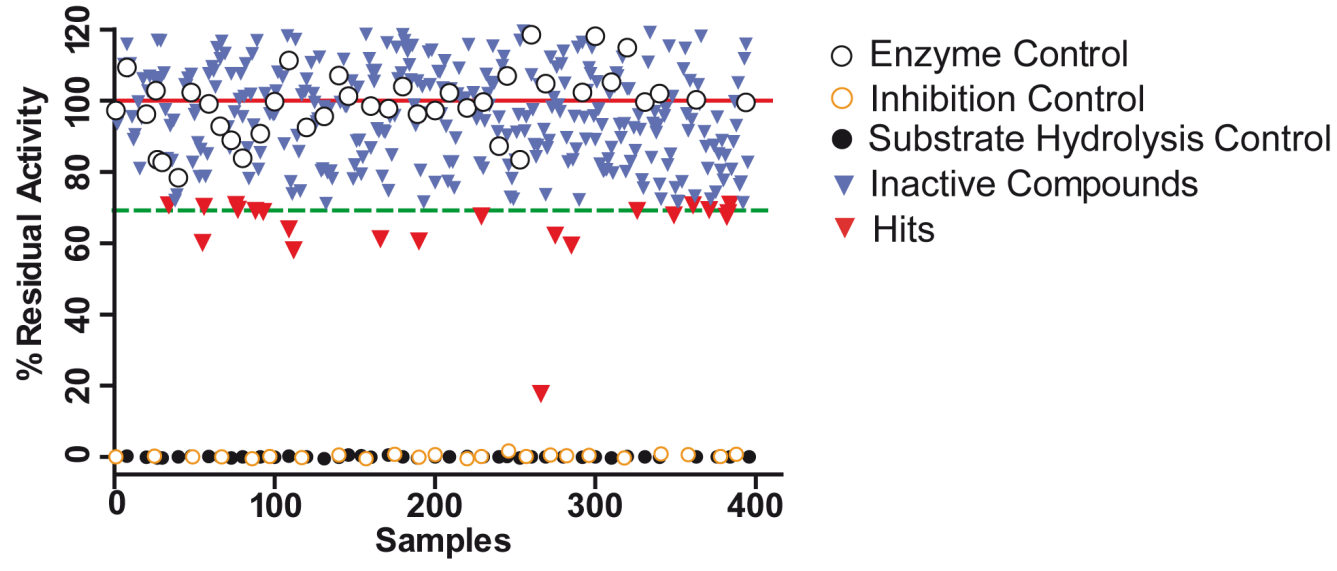808　concentration is expressed in M.

809　**Fig 8. Activity of HTS01959 on cultured *T. brucei* BSF and VERO cells.** (A)
810　Dose-response curve for *T. brucei* bloodstream forms treated with HTS01959
811　or nifurtimox as control. Viability was determined in triplicates using the
812　resazurin method. Average±SD. For each curve, the dotted line represents the
813　best fit of the four-parameter Hill equation to experimental data (open figures).
814　(B) Drug efficacy against *T. cruzi* intracellular amastigotes. The number of
815　infected cells and the number of amastigotes per cell (average ±SD) were
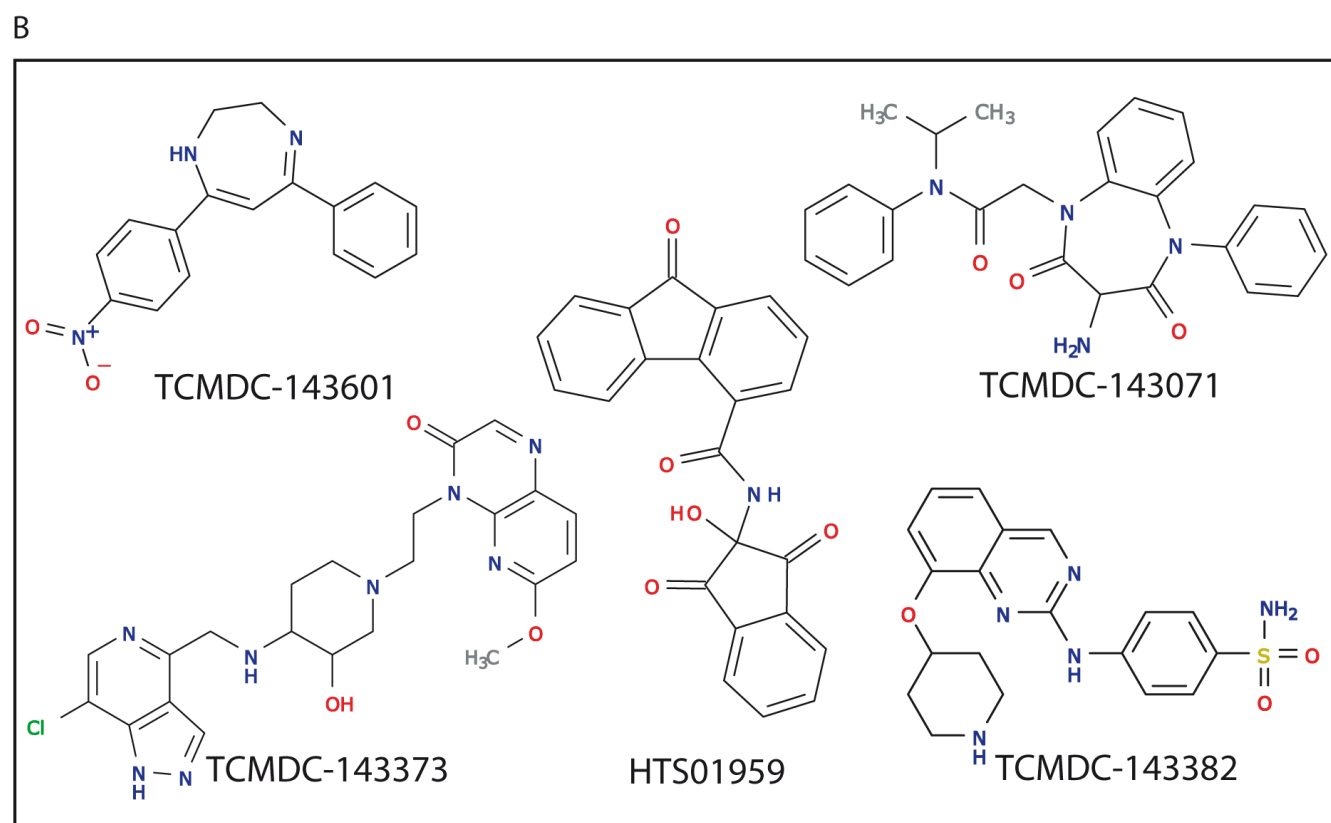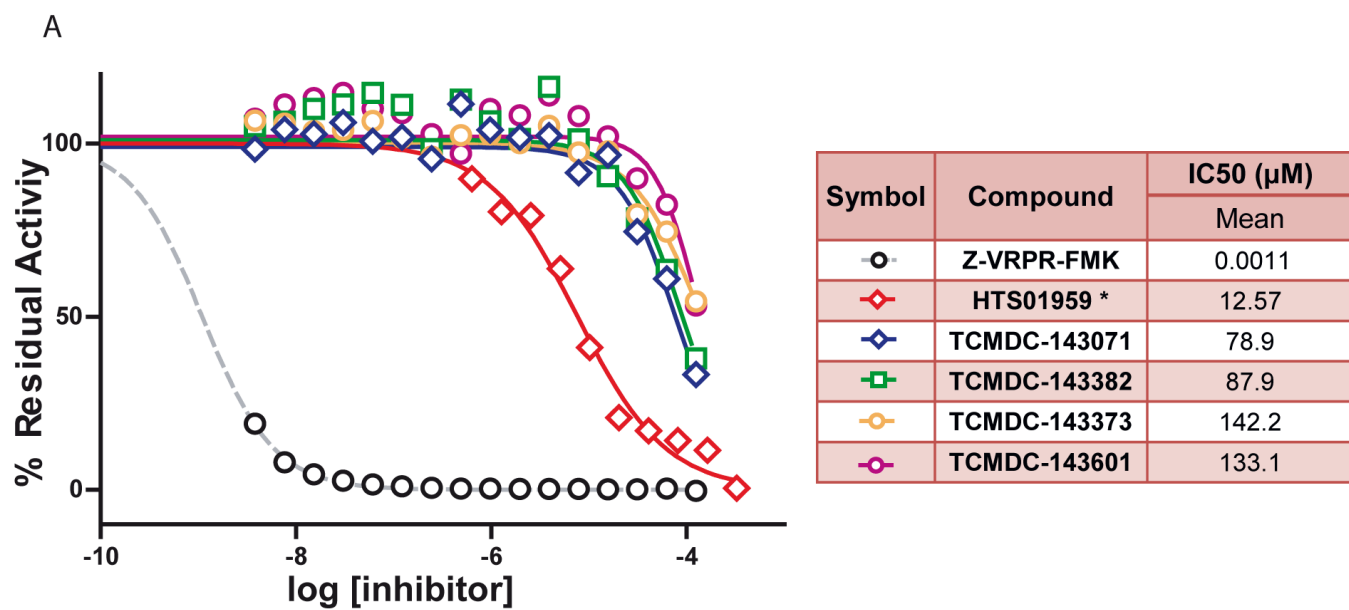816　determined by DAPI staining after 2 days of treatment with 130 μM HTS01959,

817   4 µM benznidazole as a reference inhibitor or 0.5 % v/v DMSO as control. (C)

818   Dose-response curve for *T. cruzi* trypomastigotes with HTS01959. Viability was

819   determined in triplicates using the resazurin method. Average±SD. For each

820   curve, the dotted line represents the best fit of the four-parameter Hill equation

821   to experimental data (open figures). (D) Cytotoxicity assay on VERO cells

822   treated with HTS01959 and DMSO (0.5 % v/v) as growth control. Viability was

823   determined in triplicates using a luminescent assay. Average±SD. In all cases
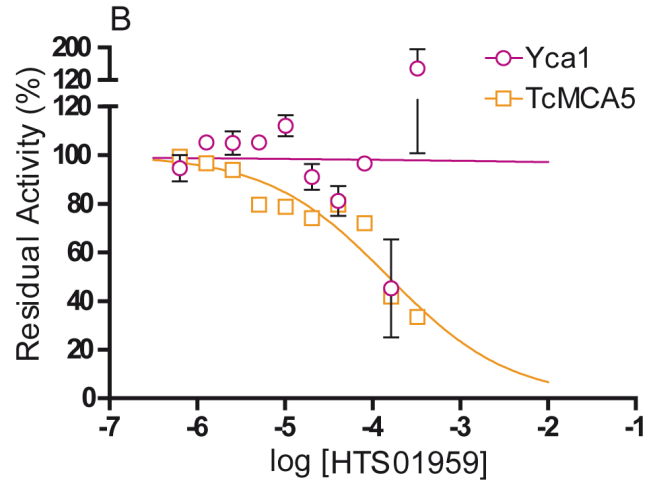
824   HTS01959 concentration is expressed in M.
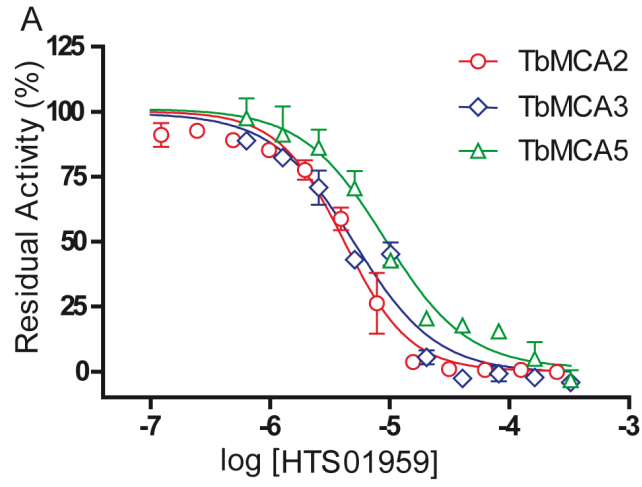
825

Enzyme	Source	Substrate	Ex/Em Wavelength	Classic Inhibitor
*Tb*MCA2	Recombinant	Z-VRPR-(AMC)	350/460	Z-VRPR-FMK
*Tb*MCA3				
*Tb*MCA5				
*Tc*MCA5				
Yca1				
Cruzipain	Natural	Z-FR-(AMC)		E64
Falcipain-2	Recombinant			
Chymotrypsin	Commercial	Suc-AAPF-(AMC)		PMSF
ACE	Commercial	Abz-FRK-(DPN)-P-OH	320/420	Captopril
Pepsin	Commercial	Moc-Ac-APAKFFRLK-(DPN)-NH2	330/393	Pepstatin

A

Symbol	Compound	IC50 (µM)
		Mean
‑‑o‑‑	Z-VRPR-FMK	0.0011
◇	HTS01959 *	12.57
◇	TCMDC-143071	78.9
□	TCMDC-143382	87.9
○	TCMDC-143373	142.2
○	TCMDC-143601	133.1

B

TCMDC-143601

TCMDC-143071

TCMDC-143373

HTS01959

TCMDC-143382

A

B

C

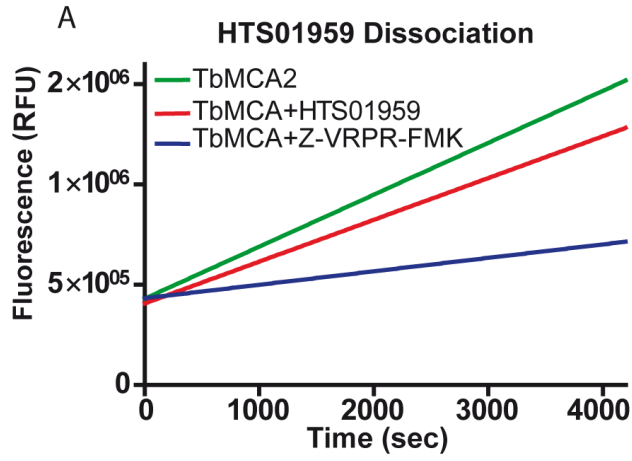| Enzyme	IC50 (µM)		HillSlope		R^2
	Mean	95 % C.I	Mean	S.E	
*Tb*MCA2	4.14	3.52 - 4.87	-1.577	0.17	0.9741
*Tb*MCA3	5.04	3.92 - 6.50	-1.265	0.1585	0.9528
*Tb*MCA5	14.39	10.01 - 16.53	-1.192	0.1744	0.8976
*Tc*MCA5	151.6	81.37 - 282.30	-0.6281	0.114	0.8887
Yca1	ND	ND	ND	ND	ND

A

HTS01959 Dissociation

TbMCA2
TbMCA+HTS01959
TbMCA+Z-VRPR-FMK

Fluorescence (RFU)

Time (sec)

B

HTS01959 Association

TbMCA2
TbMCA2+HTS01959
Initial Velocity
Steady Velocity

Fluorescence (RFU)

Time (sec)

C

Residual Activity (%)

log [HTS01959]

[Substrate](mM)
2.5
2.0
1.5
1.0
0.5
0.25
0.125
0.0625

D

IC50 (uM)

Substrate (mM)

A

B

C
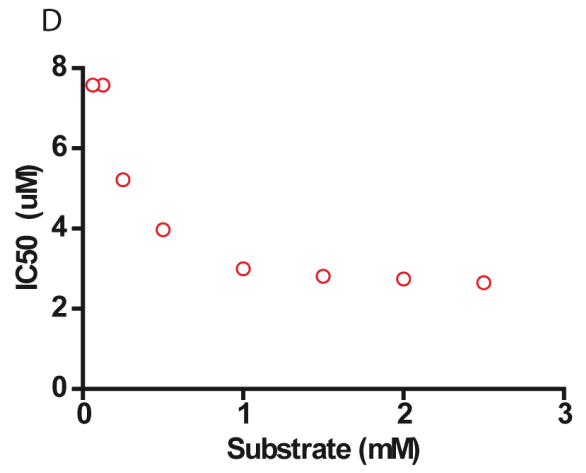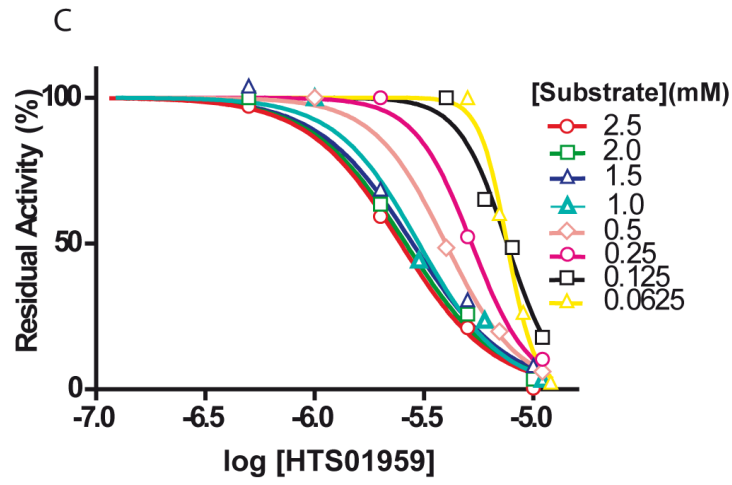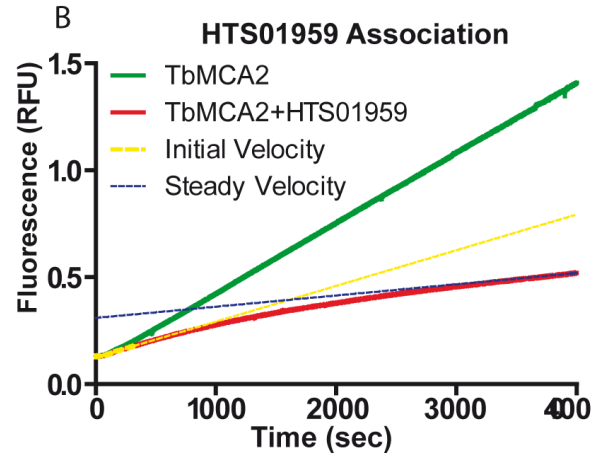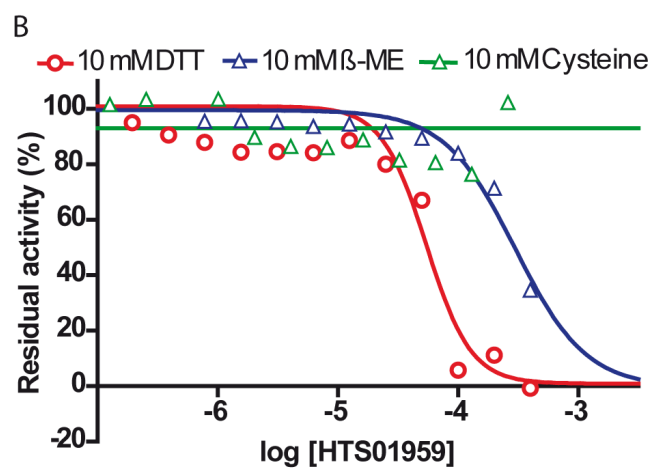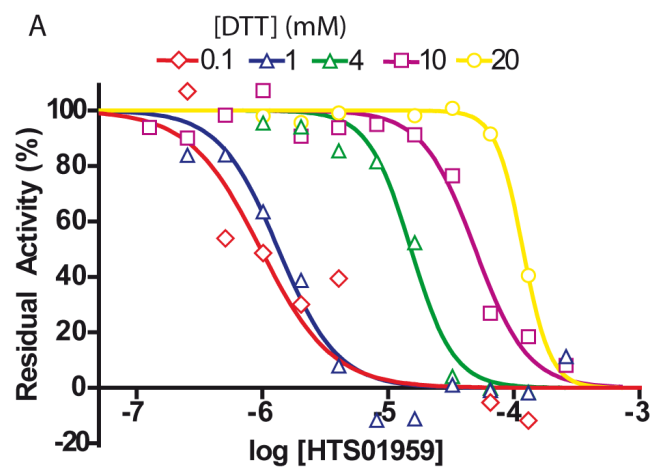
TbMCA2	IC50 (µM)		HillSlope		R^2
	Mean	95 % C.I	Mean	S.E	
DTT 0.1 mM	0.97	0.34 - 2.7	-1.534	0.978	0.712
DTT 1.0 mM	1.34	0.99 - 1.81	-1.846	0.405	0.948
DTT 4.0 mM	15.2	12.19 - 18.96	-2.558	0.531	0.978
DTT 10 mM	49.17	39.30 - 61.51	-2.082	0.384	0.962
DTT 20 mM	118.1	111.2 - 125.6	-4.013	0.465	0.99
Cysteine 0.1 mM	33.03	15.5 - 70.42	-3.08	4.147	0.7573
Cysteine 1.0 mM	89.94	28.09 - 287.9	-3.15	2.9	0.4249
Cysteine 10 mM	N. I.	N. I.	N. I.	N. I.	N. I.
β-met 10 mM	299.5	231.7 - 387.3	-1.474	0.2593	0.927

A   **Hydrogen peroxide generation**

B

A *T. brucei* **bloodstream form**

○ Nifurtimox   ○ HTS01959

B *T. cruzi* **Amastigote replication**

C *T. cruzi* **trypomastigotes**

☐ *T. cruzi* CI Brener

IC50= 91.2 μM

D **Toxicity in VERO cells**

☐ Vero - HTS01959